Broadband Absorbing Semiconducting Polymer Nanoparticles for Photoacoustic Imaging in Second Near-Infrared Window

Jiang, Yuyan; Upputuri, Paul Kumar; Xie, Chen; Lyu, Yan; Zhang, Lulu; Xiong, Qihua; Pramanik, Manojit; Pu, Kanyi

2017

Jiang, Y., Upputuri, P. K., Xie, C., Lyu, Y., Zhang, L., Xiong, Q., et al. (2017). Broadband Absorbing Semiconducting Polymer Nanoparticles for Photoacoustic Imaging in Second Near-Infrared Window. Nano Letters, 17(8), 4964-4969.

https://hdl.handle.net/10356/84411

https://doi.org/10.1021/acs.nanolett.7b02106

Broadband Absorbing Semiconducting Polymer Nanoparticles for Photoacoustic Imaging in Second Near-Infrared Window

Yuyan Jiang[†‡], *Paul Kumar Upputuri*[†‡], *Chen Xie*[†], *Yan Lyu*[†], *Lulu Zhang*[§], *Qihua Xiong*[§], *Manojit Pramanik*[†]*, *and Kanyi Pu*[†]*

[†]School of Chemical and Biomedical Engineering, Nanyang Technological University, 70 Nanyang Drive, 637459, Singapore

[§]Division of Physics and Applied Physics, School of Physical and Mathematical Sciences, Nanyang Technological University, 637371, Singapore

ABSTRACT: Photoacoustic (PA) imaging holds great promise for preclinical research and clinical practice. However, most studies rely on the laser wavelength in the first near infrared (NIR) window (NIR-I, 650-950 nm), while few studies have been exploited in the second NIR window (NIR-II, 1000-1700 nm), mainly due to the lack of NIR-II absorbing contrast agents. We herein report the synthesis of a broadband absorbing PA contrast agent based on semiconducting polymer nanoparticles (SPN-II) and apply it for PA imaging in NIR-II window. SPN-II can absorb in both NIR-I and NIR-II regions, providing the feasibility to directly compare PA imaging at 750 nm with that at 1064 nm. Due to the weaker background PA signals from biological tissues in NIR-II window, the signal-to-noise ratio (SNR) of SPN-II resulted PA images at 1064 nm can be 1.4-times higher than that at 750 nm when comparing at the imaging depth of 3 cm. The proof-of-concept application of NIR-II PA imaging is demonstrated in *in vivo* imaging of brain vasculature in living rats, which showed 1.5-times higher SNR as compared with NIR-I PA imaging. Our study not only introduces the first broadband absorbing organic contrast agent that is applicable for PA imaging in both NIR-I and NIR-II windows, but also reveals the advantages of NIR-II over NIR-I in PA imaging.

KEYWORDS: polymer nanoparticles, photoacoustic imaging, second near-infrared window, brain imaging

Photoacoustic (PA) imaging, which capitalizes on PA effect that converts absorbed photons into acoustic waves, has emerged as a promising non-invasive imaging modality for pre-clinical and clinical investigations.[1-4] As a hybrid of optical and ultrasound imaging, PA imaging breaks the optical diffusion limit, providing images with high contrast and high spatial resolution at several centimetres of tissue imaging depth.[5,6] Current PA imaging mainly utilizes near-infrared (NIR) light with the wavelengths ranging from 650 to 950 nm, while few studies have been exploited beyond 950 nm.[7-17] However, very recent studies on fluorescence imaging have identified a new imaging window termed as the second NIR (NIR-II) window (1000-1700 nm).[18-21] As compared with the first NIR (NIR-I) window (650-950 nm), fluorescence imaging in the NIR-II window affords reduced photon scattering in biological tissues and lower tissue background, leading to enhanced imaging fidelity.[22-24] In view of the lower photon energy at longer wavelength and commercial availability of cheaper, and more compact 1064 nm Nd: YAG laser (compared to laser available in the first NIR-I window), it is envisioned that PA imaging in the NIR-II window could bring about further improved imaging performance.

The key challenge to fulfil NIR-II PA imaging lies in the development of imaging agents that can efficiently absorb NIR-II light, because endogenous substances in living organisms have little absorption in this region. However, few exogenous agents can absorb in the NIR-II window, which has only been reported for copper sulfide nanoparticles,[25,26] silver nanoplates,[22] gold nanorods,[27] and phosphorous phthalocyanine.[28,29] Although semiconducting polymer nanoparticles (SPNs) have been utilized for NIR-II fluorescence imaging,[30] their application for NIR-II PA imaging has not been demonstrated so far. SPNs are mainly composed of organic semiconducting polymers with highly electron-delocalized backbones, and have formed a new class of optical agents.[30-37] Recently, we revealed that SPNs can efficiently convert photon energy into heat, permitting

photothermal cancer therapy,[38,39] and photoacoustic imaging of tumor,[40-44] lymph node,[45] and biomarkers in living animals.[46-49] Particularly, SPNs often possess higher absorption and photothermal conversion efficiencies as compared with other inorganic nanoparticles such as gold nanorods and carbon nanotubes.[41,45] These preliminary studies imply that SPNs could be promising for NIR-II PA imaging, which however is challenging in terms of chemistry design and remains to be revealed.

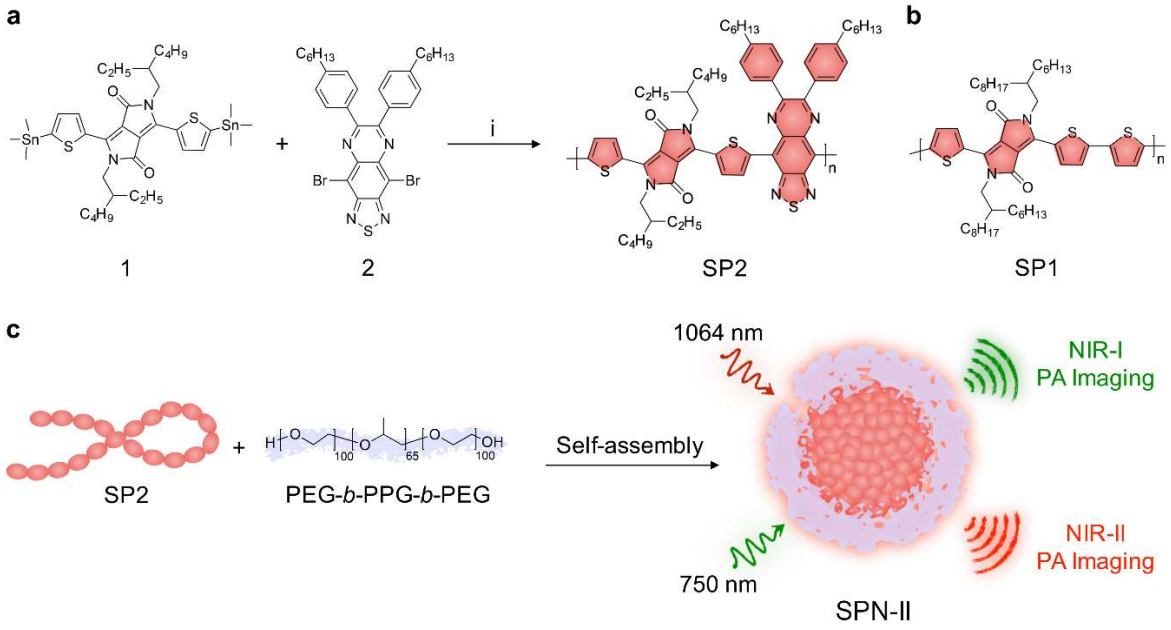

Figure 1. Preparation of SP2 and SPNs. (a) Synthetic route of SP2. (i) $PdCl_2$ $(PPh_3)_2$ and 2,6-di-*tert*-butylphenol, 100 ºC, 4 h (b) Chemical structure of SP1. (c) Schematic illustration for preparation of SPN-II *via* nanoprecipitation method.

In this study, we design and synthesize the first organic imaging agent based on SPN (SPN-II) that absorbs both NIR-I and NIR-II light and apply it for NIR-II PA imaging. The broadband absorption of SPN-II allows us to directly compare NIR-II *vs* NIR-I PA imaging so as to find out the advantages of NIR-II light in PA imaging. In the following, the molecular design principle and chemistry of SPN-II are first described along with its counterpart NIR-I light absorbing SPN (SPN-

I), followed by the study on their optical and PA properties. Then, SPN-II is used for the comparison studies between NIR-II and NIR-I PA in deep-tissue imaging. At last, the proof-of-concept application of SPN-II for NIR-II PA imaging is demonstrated in *in vivo* imaging of brain vasculatures in living rats.

To obtain broadband absorption ranging from NIR-I to NIR-II window, a new polymer, poly(diketopyrrolopyrrole-*alt*-thiadiazoloquinoxaline), (SP2, Figure 1a) was synthesized by Stille polymerization between monomers 1 and 2. In comparison with its analogue poly[diketopyrrolopyrrole-*alt*-thiophene] (SP1, Figure 1b) with an electron donor-acceptor (D-A) alternating backbone structure, SP2 had a D-A_1-D-A_2 structure, wherein thiophene was the eletron donor and both pyrrolo[3,4-c]pyrrole-1,4(2H,5H)-dione and thiadiazoloquinoxaline were the electron acceptors.[50,51] Because of the much stronger electron-withdrawing ability of thiadiazoloquinoxaline, it further lowered down the band gap, leading to the absorption in the NIR-II window. SP1 and SP2 were respectively encapsulated into an amphiphilic copolymer (PEG-*b*-PPG-*b*-PEG) via self-assembly to endow SPNs with good water-solubility (Figure **1c**). Both SPNs had the spherical morphology as indicated by transmission electron microscope (TEM) (Figure 2b), while dynamic light scattering (DLS) revealed the average diameters of SPN-I and SPN-II are 11 and 54 nm, respectively (Figure 2a). The larger diameter of SPN-II relative to SPN-I should be attributed to the steric hindrance caused by the relatively bulky size of thiadiazoloquinoxaline units. Solutions of SPNs remained clear for months and no obvious change in sizes was observed, indicating their good stability in aqueous solution (Figure 2c).

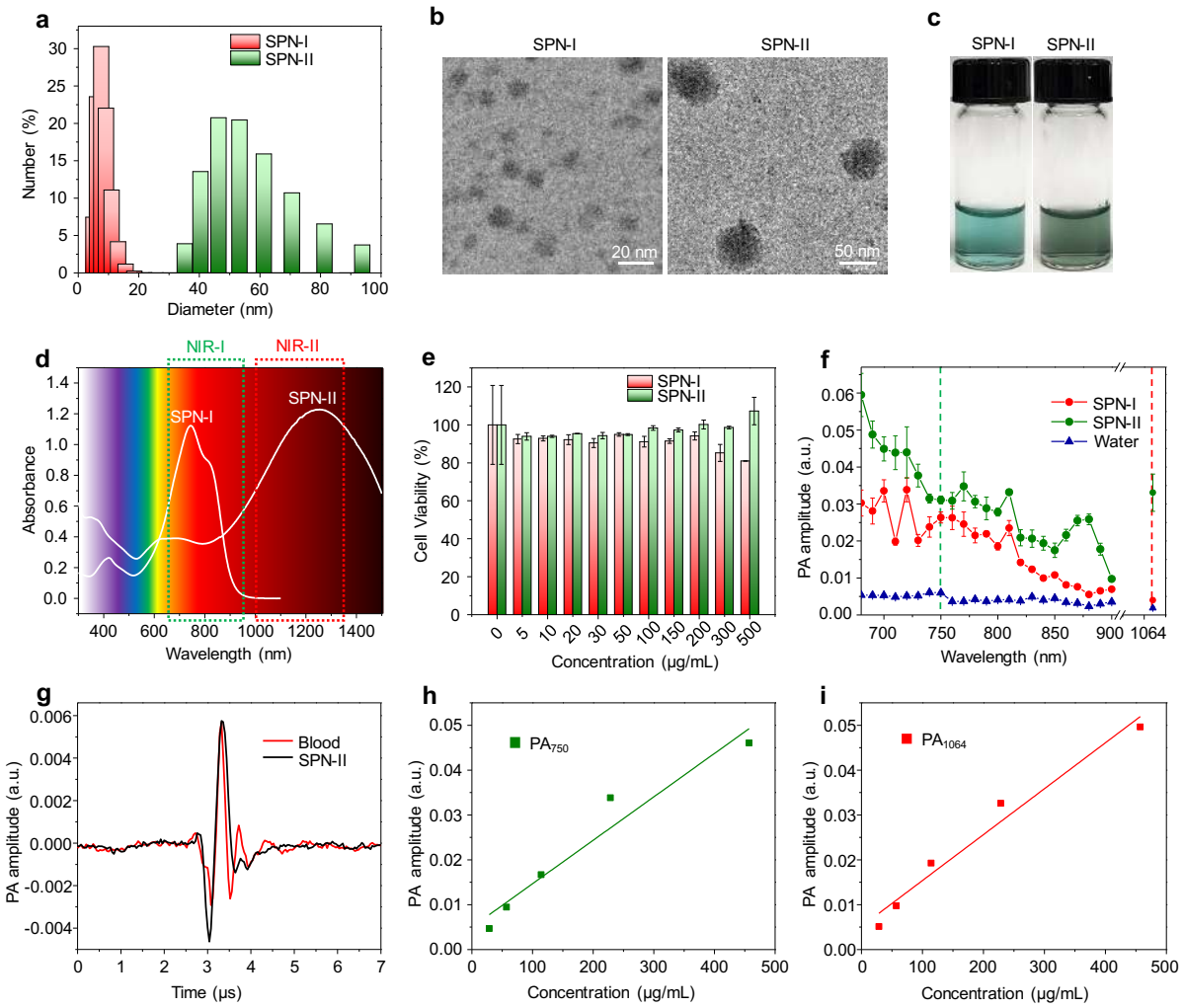

Figure 2. *In vitro* characterization of SPNs in 1 × PBS (pH = 7.4). (a) Representative DLS profiles of SPN-I and SPN-II. (b) TEM images of SPN-I and SPN-II. (c) Photographs of SPN solutions (15 μg/mL). (d) UV-Vis-NIR absorption spectra of SPN-I and SPN-II (40 μg/mL). (e) Cell viability of NIH/3T3 cells after incubation with SPNs at different concentrations. (f) PA spectra of SPNs (200 μg/mL). Error bars indicate standard deviations of 10 separate measurements. (g) Comparison of a single PA pulse generated by SPN-II (50 μg/mL) with that of blood at 1064 nm. (h) PA amplitude of SPN-II at 750 nm as a function of concentration. R^2 = 0.92667. (i) PA amplitude of SPN-II at 1064 nm as a function of concentration. R^2 = 0.96131.

Optical properties of SPNs were studied and compared under physiological conditions. The absorption of SPN-I was limited to the NIR I window with the maximum absorption at 744 nm

(Figure 2d). As expected, owning to the enhanced charge transfer caused by thiadiazoloquinoxaline with high electron deficiency, SPN-II had a broadband absorption spectrum ranging from visible to NIR II region with the maximum peak at 1253 nm.

Due to their different absorption properties, the PA spectra of SPN-I and SPN-II differed from each other (Figure 2f). SPN-II exhibited strong PA signals in both NIR I and II windows while SPN-I only generated high PA signals in the NIR I window (Figure 2f). At the same concentration (200 μg/mL), SPN-II demonstrated overall higher PA intensity than SPN-I in the range from 680 to 900 nm. In particular, the PA signals of SPN-II at 750 nm was 1.2-fold higher as compared with that of SPN-I. Moreover, SPN-II showed nearly identical PA amplitudes at 750 nm and 1064 nm, which was different from the absorption profile. The deviation between the PA and absorption spectra profiles has been widely observed for organic agents, which should be mainly caused by two factors: (i) optical absorption and PA spectra measure different photophysical processes; and (ii) optical illumination parameters are different, high-power pulsed laser for PA spectra versus low-power continuous-wave light illumination for absorption spectra.[45] Note that the PA amplitude of water at 1064 nm was lower than that at 750 nm, implying the lower background noise in the NIR-II window. Linear correlation between the concentration of SPN-II and PA amplitudes at 750 or 1064 nm was observed (Figure 2h, i), indicating the applicability for signal quantification.

To determine the suitable concentration of SPN-II for *in vivo* experiment, the PA signals of SPN-II at both 750 and 1064 nm were compared with the signal of rat blood. The critical concentration was identified to be 50 μg/mL, wherein the PA signals of SPN-II were equal to that of rat blood (Figure 2g**)**. Cytotoxicity of SPNs was studied using fibroblast cells NIH/3T3 (Figure 2e). Both

SPNs showed negligible cytotoxicity even at the incubation concentration as high as 500 μg/mL, proving their promise for biological applications.

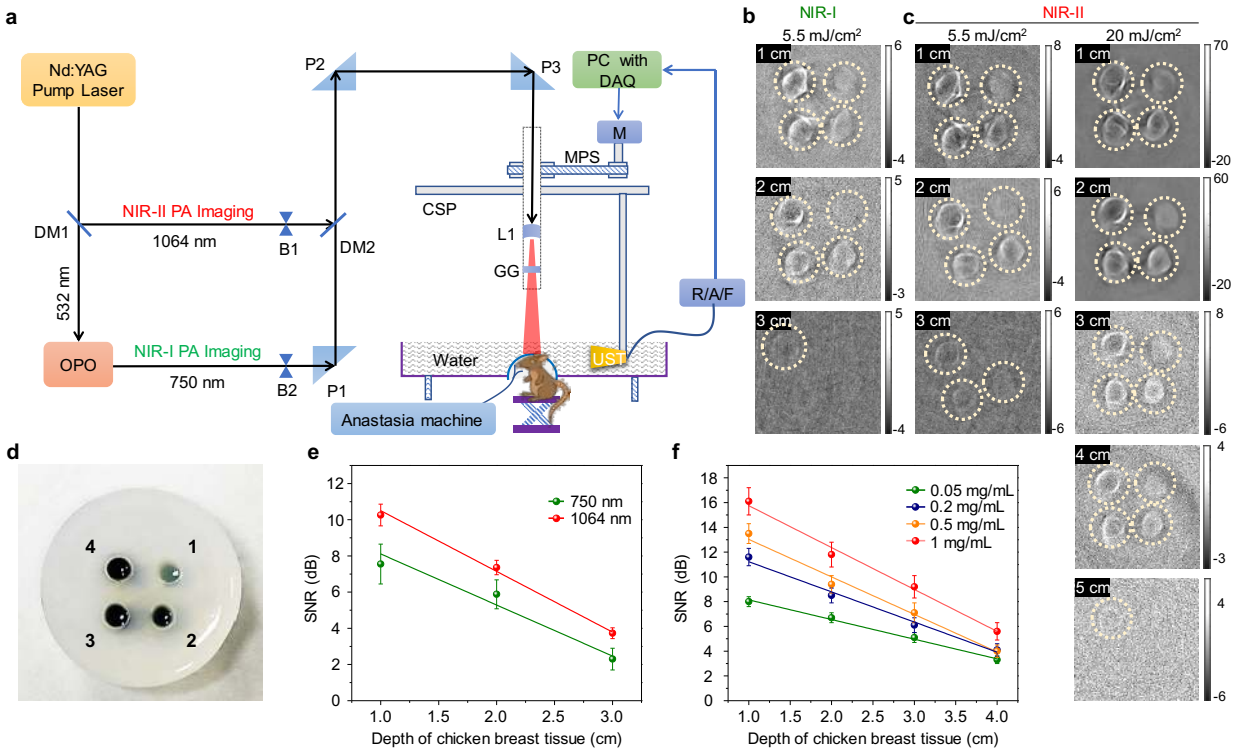

Figure 3. *Ex-vivo* Deep tissue imaging. (a) Schematic illustration of Nd:YAG/OPO PA imaging system. DM: dichromic mirror; B: beam blocker; P: antireflection coated right angle prism; MPS: motor pulley system; CSP: circular scanning plate; L1: concave lens; GG: ground glass; DAQ: data acquisition card; M: motor; R/A/F: ultrasound signal receiver, amplifier, and filter; UST: ultrasound transducer. (b) and (c) 2D PA images of the agar gel phantom containing SPN-II solutions acquired in both NIR windows at different depths. (b) NIR-I window (750 nm). Energy density: 5.5 mJ/cm^2. (c) NIR-II window (1064 nm). Left: energy density, 5.5 mJ/cm^2. Right: energy density, 20 mJ/cm^2. Scale bar: PA amplitude in mV. (d) Photograph of the agar gel phantom containing SPN-II dots with different concentrations (1-4: 0.05, 0.2, 0.5 and 1 mg/mL, respectively). (e) SNR with [SPN-II] = 1 mg/mL at 750 or 1064 nm as a function of the depth of chicken breast tissue. Energy density: 5.5 mJ/cm^2. R^2 = 0.92549 and 0.99172 for 750 and 1064 nm, respectively. (f) SNR with different SPN concentrations at 1064 nm as a function of the depth of chicken breast tissue. Energy density: 20 mJ/cm^2. R^2 = 0.99357, 0.98539, 0.98508, 0.99005 for 0.05, 0.2, 0.5 and 1 mg/mL, respectively.

To validate the advantage of SPN-II for PA imaging in the NIR II window, deep tissue imaging was conducted on a homemade bi-wavelength PA imaging system with the ability to image at both 750 and 1064 nm (Figure 3a). The solutions of SPNs with four different concentrations were embedded in an agar gel phantom and was placed under chicken breast tissues with different thicknesses (Figure 3d). To directly compare NIR-II with NIR-I imaging in terms of imaging depth, PA images were acquired at both 750 and 1064 nm with the identical laser energy density of 5.5 mJ/cm^2. At the highest concentration (1 mg/mL, spot 4), the PA signals were detectable in both NIR-I and NIR-II window at the tissue depth up to 3 cm (Figure 3b, c), which was significantly deeper as compared with fluorescence imaging (~1 mm).[2] However, signal-to-noise ratio (SNR) in decibels ($10\ln[PA_{signal}/PA_{noise}]$) for NIR-II imaging was higher than that for NIR-I imaging at all depths (Figure 3e). With decreased nanoparticle concentration, the SNR at both 750 and 1064 nm gradually decreased (Figure 3e). However, due to such a higher SNR at 1064 nm, the PA signals from SPN-II could be visualized at 3 cm with the concentration as low as 0.2 mg/mL (spot 2), which was not possible for that at 750 nm. The enhanced SNR for NIR-II PA imaging should be mainly attributed to the significantly decreased background signals in the NIR-II relative to NIR-I.[22]

Due to the relatively lower photon energy at longer wavelength, the maximum permissible exposure (MPE) increases with the laser wavelength and the MPE for skin is 100 mJ/cm^2 for 1064 nm laser, which was 25 mJ/cm^2 for 750 nm laser. We thus repeated NIR-II PA imaging experiment at 1064 nm with the increased laser energy density of 20 mJ/cm^2. As expected, imaging depth was enhanced with increased laser energy density. Particularly, 4 and 5 cm deep imaging were achieved for the lowest (0.05 mg/mL, spot 1) and highest concentration (1 mg/mL, spot 4), respectively (Figure 3f). These results demonstrated that additionally improved imaging depth could be

achieved by NIR-II vs NIR-I PA imaging owing to its higher practical MPE. In fact, PA imaging at 1064 nm has been reported to reach 11.6 cm in chicken breast tissue with the laser power of 56 mJ/cm^2.[29]

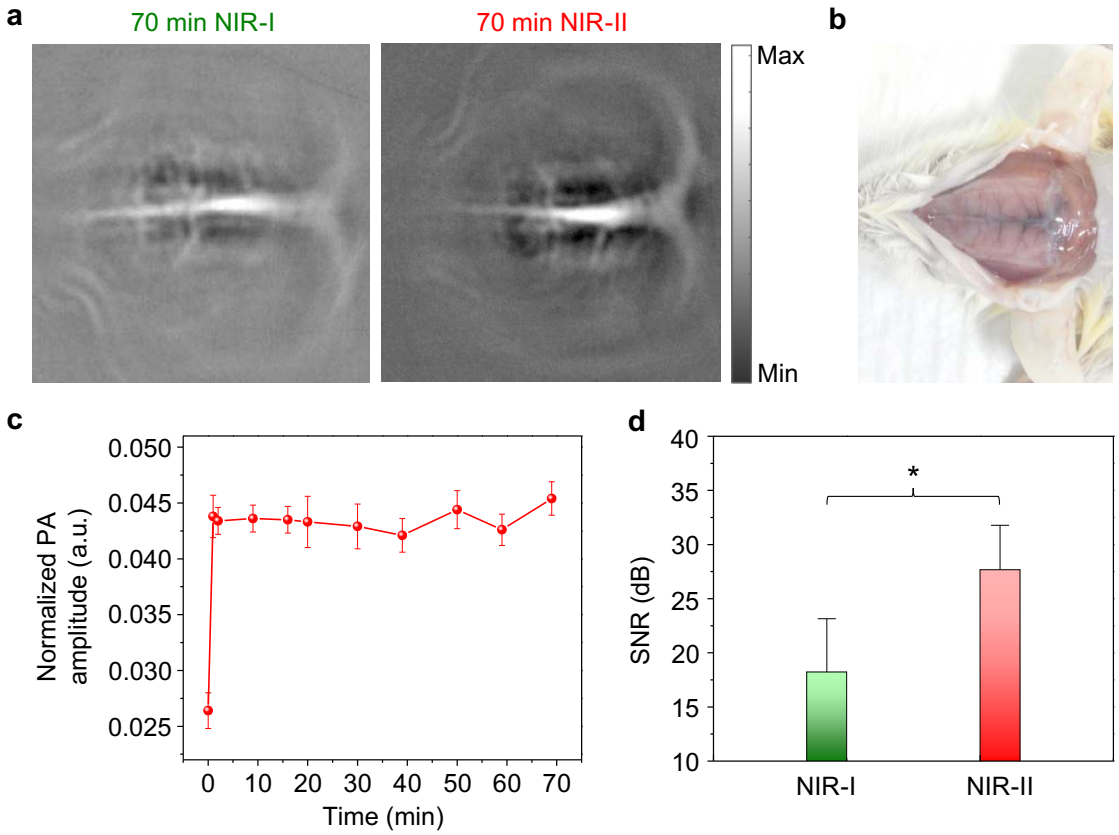

Figure 4. *In vivo* PA imaging of rat brain in both NIR-I and NIR-II window. (a) Representative PA images of rat cortex at 70 min post-injection of SPN-II at 750 nm and 1064 nm. SPN-II was administered via tail vein injection with a dose of 1.8 mg per rat (n = 3). (b) Representative photograph of cortex vessels of the same rat after PA imaging and skin removal. (c) Normalized maximum PA amplitudes as a function of time at 750 nm post-injection of SPN-II. (d) SNR in decibels of brain cortex at 70 min post-injection of SPN-II at 750 and 1064 nm. Energy density, 5.5 mJ/cm^2. *Statistically significant difference in SNR (dB) between NIR-I and NIR-II window ($p < 0.05$, $n = 3$).

To validate the PA imaging capability of SPN-II as well as to examine the merits of NIR-II *vs* NIR-I imaging, *in vivo* imaging of brain cortex in living rats was performed on the homemade bi-wavelength PA system (Figure 3a). Because the laser beam at 1064 nm was difficult to align, real-time PA images were first recorded at 750 nm. After intravenous injection of SPN-II (6 mg/mL, 300 μL per rat), the PA signals from the blood vessels were increased by 66% (Figure 4c), and the SNR at 750 nm (15.4 dB) was enhanced by about 1.5-fold, making both main and branch vessels much easier to visualize. The SNR was stabilized at about 18 dB for 70 min at least, indicting the long-circulation of SPN-II in blood owning to its small diameter (~54 nm) and PEG-passivated surface. At 70 min post injection, the PA images were recorded at both 750 and 1064 nm (Figure 4a). It is clear that the background signal at 1064 nm was lower than that at 750 nm, and the SNR at 1064 nm (27.7 ± 4.1 dB) was 1.5-fold of that at 750 nm (18.2 ± 4.9 dB) (Figure 4d). These results corresponded well with the tissue experiment and further confirmed the advantage of NIR-II over NIR-I PA imaging.

In conclusion, we have designed and synthesized a SPN-based PA contrast agent that had broadband absorption in both NIR-I and NIR-II windows. Taking advantage of pyrrolo[3,4-c]pyrrole-1,4(2H,5H)-dione and thiadiazoloquinoxaline as the first and second electron acceptors, a special D-A_1-D-A_2 structure was constructed for SP2 to enhance donor-acceptor interactions in the π-conjugated backbone and in turn narrow the band gap, ultimately red-shifting its absorption into NIR-II region. The broadband absorption allowed SPN-II to serve as both NIR-I and NIR-II PA imaging agent, which had nearly identical PA amplitudes at 750 and 1064 nm. This unique optical feature of SPN-II enabled direct comparison between NIR-I and NIR-II PA imaging. The SPN-II resulted PA images acquired at 1064 nm could exhibit 1.4-times higher SNR than that at 750 nm at the tissue depth of 3 cm, mainly owing to the decreased background PA signals of

biological tissue in NIR-II window. The proof-of-concept application of SPN-II for *in vivo* NIR-II PA imaging was demonstrated in imaging of brain vasculature in living rats, which showed a 1.5-times increase in SNR as compared with NIR-I imaging at the same laser fluence. Technically, such higher SNR of NIR-II PA imaging relative to that of NIR-I PA imaging could be further enhanced by increasing the laser power due to the higher MPE at longer wavelengths.

To the best of our knowledge, this study reveals the first organic PA agent that can generate PA signals in both NIR-I and NIR-II windows. Furthermore, we believe that this study provides the clear evidence to support that shifting PA imaging into NIR-II window is meaningful and thus highlights the necessity to develop contrast agents with the ability to generate NIR-II PA signals.

ASSOCIATED CONTENT

Supporting information

The supporting information is available free of charge. Experimental details, synthetic procedures of SP2, preparation of SPNs, characterization of SP and SPNs, *in vitro, ex vivo and in vivo* PA studies of SPNs. (Figure S1-S4 and Table S1) (PDF)

AUTHOR INFORMATION

Corresponding Author

*E-mail: kypu@ntu.edu.sg.

*E-mail: manojit@ntu.edu.sg.

Author Contributions

The manuscript was written through contributions of all authors. All authors have given approval to the final version of the manuscript. ‡These authors contributed equally.

Notes

The authors declare no competing financial interest.

ACKNOWLEDGEMENTS

K.P. thanks Nanyang Technological University (Start-Up grant: NTU-SUG: M4081627.120) and Singapore Ministry of Education (Academic Research Fund Tier 1: RG133/15 M4011559 and Academic Research Fund Tier 2 MOE2016-T2-1-098) for the financial support. M. P . thanks the Singapore Ministry of Health's National Medical Research Council (NMRC/OFIRG/0005/2016: M4062012) for the financial support.

REFERENCES

(1) Ntziachristos, V. *Nat. Meth.* **2010**, *7*, 603-614.
(2) Wang, L. V.; Yao, J. *Nat. Meth.* **2016**, *13*, 627-638.
(3) Li, L.; Zhu, L.; Ma, C.; Lin, L.; Yao, J.; Wang, L.; Maslov, K.; Zhang, R.; Chen, W.; Shi, J.; Wang, L. V. *Nature Biomedical Engineering* **2017**, *1*, 0071.
(4) Upputuri, P. K.; Pramanik, M. *J. Biomed. Opt.* **2017**, *22*, 041006.
(5) Kim, C.; Favazza, C.; Wang, L. V. *Chem. Rev.* **2010**, *110*, 2756-2782.
(6) Wang, L. V.; Hu, S. *Science* **2012**, *335*, 1458.
(7) Chen, Q.; Liu, X.; Chen, J.; Zeng, J.; Cheng, Z.; Liu, Z. *Adv. Mater.* **2015**, *27*, 6820-6827.
(8) Fan, Q.; Cheng, K.; Hu, X.; Ma, X.; Zhang, R.; Yang, M.; Lu, X.; Xing, L.; Huang, W.; Gambhir, S. S. *J. Am. Chem. Soc.* **2014**, *136*, 15185-15194.
(9) Wang, J.; Chen, F.; Arconada-Alvarez, S. J.; Hartanto, J.; Yap, L.-P.; Park, R.; Wang, F.; Vorobyova, I.; Dagliyan, G.; Conti, P. S.; Jokerst, J. V. *Nano Lett.* **2016**, *16*, 6265-6271.
(10) Smith, B. R.; Gambhir, S. S. *Chem. Rev.* **2017**, *117*, 901-986.
(11) Chen, Q.; Liang, C.; Sun, X.; Chen, J.; Yang, Z.; Zhao, H.; Feng, L.; Liu, Z. *Proc. Nat. Acad. Sci.* **2017**, 201701976.
(12) Manohar, S.; Vaartjes, S. E.; Hespen, J. C. G. v.; Klaase, J. M.; Engh, F. M. v. d.; Steenbergen, W.; Leeuwen, T. G. v. *Opt. Express* **2007**, *15*, 12277-12285.
(13) Ermilov, S. A.; Khamapirad, T.; Conjusteau, A.; Leonard, M. H.; Lacewell, R.; Mehta, K.; Miller, T.; Oraevsky, A. A. *J. Biomed. Opt.* **2009**, *14*, 024007.
(14) Wang, L. V. *Nat. Photon.* **2009**, *3*, 503-509.
(15) Weber, J.; Beard, P. C.; Bohndiek, S. E. *Nat. Meth.* **2016**, *13*, 639-650.
(16) Fan, Q.; Cheng, K.; Yang, Z.; Zhang, R.; Yang, M.; Hu, X.; Ma, X.; Bu, L.; Lu, X.; Xiong, X.; Huang, W.; Zhao, H.; Cheng, Z. *Adv. Mater.* **2015**, *27*, 843-847.
(17) Ntziachristos, V.; Razansky, D. *Chem. Rev.* **2010**, *110*, 2783-2794.

(18) Antaris, A. L.; Chen, H.; Cheng, K.; Sun, Y.; Hong, G.; Qu, C.; Diao, S.; Deng, Z.; Hu, X.; Zhang, B.; Zhang, X.; Yaghi, O. K.; Alamparambil, Z. R.; Hong X.; Cheng, Z; Dai, H. *Nat. Mater.* **2016**, *15*, 235-242.
(19) Shou, K.; Qu, C.; Sun, Y.; Chen, H.; Chen, S.; Zhang, L.; Xu, H.; Hong, X.; Yu, A.; Cheng, Z. *Adv. Funct. Mater.* **2017**, 1700995.
(20) Yang, Q.; Ma, Z.; Wang, H.; Zhou, B.; Zhu, S.; Zhong, Y.; Wang, J.; Wan, H.; Antaris, A.; Ma, R.; Zhang, X.; Yang, J.; Zhang, X.; Sun, H.; Liu, W.; Liang, Y.; Dai, H. *Adv. Mater.* **2017**, *29*, 1605497.
(21) Zhu, S.; Yang, Q.; Antaris, A. L.; Yue, J.; Ma, Z.; Wang, H.; Huang, W.; Wan, H.; Wang, J.; Diao, S.; Zhang, B.; Li, X.; Zhong, Y.; Yu, K.; Hong, G.; Luo, J.; Liang, Y.; Dai, H. *Proc. Nat. Acad. Sci.* **2017**, 201617990.
(22) Homan, K.; Kim, S.; Chen, Y.-S.; Wang, B.; Mallidi, S.; Emelianov, S. *Opt. Lett.* **2010**, *35*, 2663-2665.
(23) Hong, G.; Antaris, A. L.; Dai, H. *Nature Biomedical Engineering* **2017**, *1*, 0010.
(24) Smith, A. M.; Mancini, M. C.; Nie, S. *Nat. Nano.* **2009**, *4*, 710-711.
(25) Ku, G.; Zhou, M.; Song, S.; Huang, Q.; Hazle, J.; Li, C. *ACS Nano* **2012**, *6*, 7489-7496.
(26) Zhou, M.; Ku, G.; Pageon, L.; Li, C. *Nanoscale* **2014**, *6*, 15228-15235.
(27) Chen, Y.-S.; Homan, K.; Xu, D.; Frey, W.; Emelianov, S. *Biomedical Optics and 3-D Imaging; Optical Society of America: Miami, Florida* **2012**, BM2B.7.
(28) Hannah, A. S.; VanderLaan, D.; Chen, Y.-S.; Emelianov, S. Y. *Biomed. Opt. Express* **2014**, *5*, 3042-3052.
(29) Zhou, Y.; Wang, D.; Zhang, Y.; Chitgupi, U.; Geng, J.; Wang, Y.; Zhang, Y.; Cook, T. R.; Xia, J.; Lovell, J. F. *Theranostics* **2016**, *6*, 688-697.
(30) Kuo, C.-T.; Thompson, A. M.; Gallina, M. E.; Ye, F.; Johnson, E. S.; Sun, W.; Zhao, M.; Yu, J.; Wu, I. C.; Fujimoto, B.; DuFort, C. C.; Carlson, M. A.; Hingorani, S. R.; Paguirigan, A. L.; Radich, J. P.; Chiu, D. T. *Nat. Commun.* **2016**, *7*, 11468.
(31) Feng, L.; Zhu, C.; Yuan, H.; Liu, L.; Lv, F.; Wang, S. *Chem. Soc. Rev.* **2013**, *42*, 6620-6633.
(32) Ke, C.-S.; Fang, C.-C.; Yan, J.-Y.; Tseng, P.-J.; Pyle, J. R.; Chen, C.-P.; Lin, S.-Y.; Chen, J.; Zhang, X.; Chan, Y.-H. *ACS nano* **2017**, *11*, 3166-3177.
(33) Liu, H.-Y.; Wu, P.-J.; Kuo, S.-Y.; Chen, C.-P.; Chang, E.-H.; Wu, C.-Y.; Chan, Y.-H. *J. Am. Chem. Soc.* **2015**, *137*, 10420-10429.
(34) Shuhendler, A. J.; Pu, K.; Cui, L.; Uetrecht, J. P.; Rao, J. *Nat. Biotech.* **2014**, *32*, 373-380.
(35) Sun, K.; Tang, Y.; Li, Q.; Yin, S.; Qin, W.; Yu, J.; Chiu, D. T.; Liu, Y.; Yuan, Z.; Zhang, X.; Wu, C. *ACS Nano* **2016**, *10*, 6769-6781.
(36) Wang, Y.; Li, S.; Liu, L.; Lv, F.; Wang, S. *Angew. Chem.* **2017**, *129* (19), 5392-5395.
(37) Wu, I. C.; Yu, J.; Ye, F.; Rong, Y.; Gallina, M. E.; Fujimoto, B. S.; Zhang, Y.; Chan, Y.-H.; Sun, W.; Zhou, X.-H.; Wu, C.; Chiu, D. T. *J. Am. Chem. Soc.* **2015**, *137*, 173-178.
(38) Lyu, Y.; Fang, Y.; Miao, Q.; Zhen, X.; Ding, D.; Pu, K. *ACS nano* **2016**, *10*, 4472-4481.
(39) Zhu, H.; Lai, Z.; Fang, Y.; Zhen, X.; Tan, C.; Qi, X.; Ding, D.; Chen, P.; Zhang, H.; Pu, K. *Small* **2017**, *13*, 1604139.
(40) Cui, D.; Xie, C.; Lyu, Y.; Zhen, X.; Pu, K. *J. Mat. Chem. B* **2017**, DOI: 10.1039/c6tb03393h.
(41) Pu, K.; Mei, J.; Jokerst, J. V.; Hong, G.; Antaris, A. L.; Chattopadhyay, N.; Shuhendler, A. J.; Kurosawa, T.; Zhou, Y.; Gambhir, S. S. *Adv. Mater.* **2015**, *27*, 5184-5190.
(42) Xie, C.; Upputuri, P. K.; Zhen, X.; Pramanik, M.; Pu, K. *Biomaterials* **2017**, *119*, 1-8.
(43) Xie, C.; Zhen, X.; Lei, Q.; Ni, R.; Pu, K. *Adv. Funct. Mater.* **2017**, *27*, 1605397.
(44) Zhen, X.; Feng, X.; Xie, C.; Zheng, Y.; Pu, K. *Biomaterials* **2017**, *127*, 97-106.

(45) Pu, K.; Shuhendler, A. J.; Jokerst, J. V.; Mei, J.; Gambhir, S. S.; Bao, Z.; Rao, J. *Nat. Nano.* **2014**, *9*, 233-239.
(46) Lyu, Y.; Zhen, X.; Miao, Y.; Pu, K. *ACS nano* **2016**, *11*, 358-367.
(47) Miao, Q.; Lyu, Y.; Ding, D.; Pu, K. *Adv. Mater.* **2016**, *28*, 3662-3668.
(48) Yin, C.; Zhen, X.; Fan, Q.; Huang, W.; Pu, K. *ACS nano* **2017**, *11*, 4174-4182.
(49) Zhang, J.; Zhen, X.; Upputuri, P. K.; Pramanik, M.; Chen, P.; Pu, K. *Adv. Mater.* **2016**, *29*, 1604764.
(50) Dou, L.; Liu, Y.; Hong, Z.; Li, G.; Yang, Y. *Chem. Rev.* **2015**, *115*, 12633-12665.
(51) Steckler, T. T.; Henriksson, P.; Mollinger, S.; Lundin, A.; Salleo, A.; Andersson, M. R. *J. Am. Chem. Soc.* **2014**, *136*, 1190-1193.

TOC Figure